Inorganic Chemistry

Article

pubs.acs.org/IC

The Complexation of Cm(III) with Oxalate in Aqueous Solution at T = 20−90 °C: A Combined TRLFS and Quantum Chemical Study

Andrej Skerencak-Frech,*[,†] Martin Maiwald,[‡] Michael Trumm,[†] Daniel R. Froehlich,[‡] and Petra J. Panak[‡]

[†]KIT−Campus Nord, Institut für Nukleare Entsorgung, D-76344 Eggenstein-Leopoldshafen, Germany

[‡]Ruprecht Karls Universität Heidelberg, Physikalisch-Chemisches Institut, Im Neuenheimer Feld 253, D-69120 Heidelberg, Germany

Supporting Information

ABSTRACT: The complexation of Cm(III) with oxalate is studied in aqueous solution as a function of the ligand concentration, the ionic strength (NaCl), and the temperature (T = 20−90 °C) by time-resolved laser fluorescence spectroscopy (TRLFS) and quantum chemical calculations. Four complex species ($[Cm(Ox)_n]^{3-2n}$, n = 1, 2, 3, 4) are identified, and their molar fractions are determined by peak deconvolution of the emission spectra. The conditional log $K'_n(T)$ values of the first three complexes are calculated and extrapolated to zero ionic strength with the specific ion interaction theory approach. The $[Cm(Ox)_4]^{5-}$ complex forms only at high temperatures. Thus, the log $K_4^0(T)$ value was determined at T > 60 °C. The log K_1^0(25 °C) = 6.86 ± 0.02 decreases by 0.1 logarithmic units in the studied temperature range. The log K_2^0(25 °C) = 4.68 ± 0.09 increases by 0.35, and log K_3^0(25 °C) = 2.11 ± 0.05 increases by 0.37 orders of magnitude. The log $K_n^0(T)$ (n = 1, 2, 3) values are linearly correlated with the reciprocal temperature. Thus, their temperature dependencies are fitted with the linear Van't Hoff equation yielding the standard reaction enthalpy ($\Delta_r H_m^0$) and standard reaction entropy ($\Delta_r S_m^0$) of the stepwise formation of the $[Cm(Ox)_n]^{3-2n}$ species (n = 1, 2, 3). Furthermore, the binary ion−ion interaction coefficients of the four Cm(III) oxalate species with Cl^-/Na^+ are determined. The binding energies, bond lengths, and bond angles of the different Cm(III) oxalate complexes are calculated in the gas phase as well as in a box containing 1000 H_2O molecules by ab inito calculations and molecular dynamics simulations, respectively.

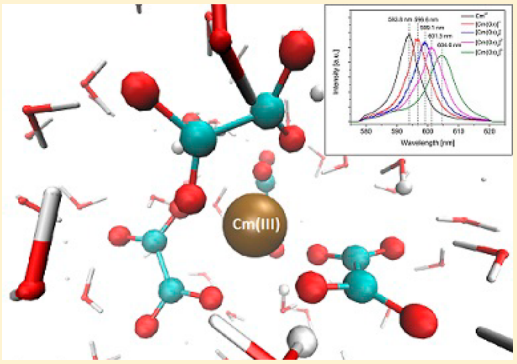

1. INTRODUCTION

One of the main safety issues of the civil application of nuclear fission for power generation is the disposal of the accumulating radioactive waste. Among unspent uranium and fission products, plutonium and the minor actinides (Np, Am, Cm) are present in the waste due to neutron capture reactions in the reactor. Some isotopes of the actinides have very long half-lives (e.g., $T_{1/2}$(Pu-239) = 2.41 × 10^4 years). Thus, the actinides will determine the radiotoxicity of the nuclear waste over very long time scales (>10^5 years). The disposal of the nuclear waste requires an effective isolation from the biosphere for a long time. The only valid option to achieve this is the storage of the waste in deep geological formations. The safety assessment of a nuclear waste repository requires the consideration of different incident scenarios, such as the intrusion of water and subsequent dissolution of the waste matrix. Thus, detailed knowledge of the aqueous geochemistry is required. Beside reactions at the liquid−solid interface (e.g., dissolution of the waste matrix, sorption to mineral surfaces, etc.), complexation reactions with different ligands in the aqueous phase are of major importance for the migration behavior of the actinides. These reactions must be described by a comprehensive thermodynamic model based on stability constants (log β_n^0) and standard reaction enthalpies ($\Delta_r H_m^0$) and entropies ($\Delta_r S_m^0$). Only by this approach reliable predictions on the migration behavior of the actinides over very long time scales can be made.

In the past, extensive work has been dedicated to determine thermodynamic data of the actinides in their most relevant oxidation states. A critical review and summary of a majority of these works is given in the OECD-NEA Thermodynamic Database.[1] However, most of the available data is limited to ambient temperatures. Because of the radioactive decay of the radionuclides and the accompanied release of heat, the temperature in the near field of a repository will increase significantly. The temperature depends on the stored waste, the geometry of the repository, and the type of host rock. In this context the question arises how and to what extent these increased temperatures will affect the thermodynamics of the actinides. To give a comprehensive long-term safety assessment of a nuclear waste repository in deep geological formations, thermodynamic data at ambient temperatures as well as at T > 25 °C is needed.

The present work focuses on the complexation of Cm(III) with oxalate at T = 20−90 °C. Because of the chemical similarities of trivalent actinides and the outstanding spectroscopic properties of Cm(III), this element is used as an

Received: November 14, 2014
Published: February 3, 2015

DOI: 10.1021/ic502749x
Inorg. Chem. 2015, 54, 1860−1868

analogue for Am(III) and Pu(III). Studies on Am oxalate complexes are of particular interest for two reasons. First, oxalic acid is widely applied in obtaining oxides of different actinides. For example, the main conversion route of elemental plutonium into its oxide is oxalic conversion (e.g., AREVAs spent nuclear fuel recycling plant in La Hague).[2−4] Thus, oxalate may be present in high concentration in liquid nuclear waste (e.g., the total amount of Na_2Ox and H_2Ox in the WIPP repository is expected to be ∼50 tons).[5] Furthermore, oxalate is present in natural systems, such as brines in oil field sedimentary basins or soil solutions. These deposits originate from the thermal decomposition of more complex organic matter.[6] The formation of oxalate complexes of the actinides may result in an increased solubility of the waste matrix. Furthermore, studies on the complexation of actinides with small organic ligands provide fundamental information on the mechanism of these complexation reactions and may contribute to a better understanding of the complexation properties of more complex organic macromolecules (e.g., humic acids).

2. EXPERIMENTAL SECTION

2.1. Sample Preparation. All samples were prepared on a molal concentration scale (mol/kg H_2O, "m") to avoid variation of the concentration due to changes of solution density with increasing temperature and increasing ionic strength. The concentration of Cm(III) in all samples was fixed at 5×10^{-9} m by adding a defined quantity of a Cm(III) stock solution ($[Cm(III)]_{stock} = 1 \times 10^{-7}$ m (isotopic composition: 89.7% Cm-248, 9.4% Cm-246, <0.9% Cm-243, Cm-245, and Cm-247).

Ten samples with different total oxalate concentrations ($[Ox^{2-}]_{tot}$ = (0.47−7.55)·× 10^{-3} m) were prepared. The ionic strength of the samples was increased successively from I_m = 1.0−4.0 by adding solid NaCl (Merck, Suprapure). The total proton concentration in each sample was fixed at $[H^+]_{tot} = 9.31 \times 10^{-3}$ m with HCl (Merck, Titrisol). Additional details on the pH of the samples are given in the Supporting Information. The temperature of each sample was increased successively from 20 to 90 °C, and an emission spectrum was recorded at each single temperature. The emission spectra of the samples were compared before and after heating. In each case total reversibility was observed. This ensures that the samples are in thermodynamic equilibrium and that no irreversible reactions (e.g., precipitation) occur.

The concentrations of the different oxalate species (H_2Ox, HOx^-, Ox^{2-}, $NaOx^-$) at equilibrium conditions were calculated with the software Hyperquad HySS (Version 4.0.31[7]) as a function of $[Ox^{2-}]_{tot}$, $[H^+]_{tot}$, I_m, and T. The calculations are based on the following chemical model and thermodynamic constants:[1,8−10]

$$Ox^{2-} + H^+ \rightleftharpoons HOx^-$$
$$\log \beta_1^0(25°C) = 4.25 \pm 0.01; \Delta_r H_m^0 = 7.3 \pm 0.1 \text{ kJ/mol}$$

$$Ox^{2-} + 2H^+ \rightleftharpoons H_2Ox$$
$$\log \beta_2^0(25°C) = 5.65 \pm 0.06; \Delta_r H_m^0 = 10.6 \pm 0.6 \text{ kJ/mol}$$

$$Na^+ + Ox^{2-} \rightleftharpoons NaOx^-$$
$$\log \beta_3^0(25°C) = 1.10 \pm 0.01; \Delta_r H_m^0 = -5.0 \pm 0.7 \text{ kJ/mol}$$

The temperature-dependent thermodynamic stability constants ($\log \beta_x^0(T)$) were calculated with the linear Van't Hoff equation.[11] The activity coefficients for the different ionic species ($\gamma_i(T)$) and the conditional stability constants ($\log \beta'_x(T)$) were calculated according to the specific ion interaction theory approach, using the binary ion−ion interaction coefficients given in the Nuclear Energy Agency Thermochemical Database (NEA-TDB) ($\varepsilon(H^+,Cl^-) = 0.12 \pm 0.01$, $\varepsilon(Na^+,HOx^-) = -0.07 \pm 0.01$, $\varepsilon(Na^+,Ox^{2-}) = -0.08 \pm 0.01$, $\varepsilon(Na^+,NaOx^-) \approx \varepsilon(Na^+,HOx^-) = -0.07 \pm 0.01$).[1] A detailed summary of the calculated $\log \beta'(T)$ values is given in the Supporting Information.

2.2. Time-Resolved Laser Fluorescence Spectroscopy. TRLFS measurements were performed with a pulsed Nd:YAG (Surelite II, Continuum, USA) pumped dye laser (NarrowScan, Radiant Dyes Laser & Accessories GmbH, Germany) with a pulse energy between 2 and 4 mJ. The temperature was controlled by a thermostat (K6-mpc-NR, Peter Huber Kältemaschinenbau GmbH, Germany). Curium was excited at 396.6 nm. The detector system consists of an iStar Gen II ICCD camera and a Shamrock SR-303i imaging spectrograph (both ANDOR Technology PLC, Northern Ireland) with a 1200 lines/mm grating and a spectral range of 580−620 nm. The spectra were measured in time-gated detection mode with an initial delay of 1 μs and a gate width of 1 ms. Details on the experimental setup are given elsewhere.[12]

2.3. Theoretical Models. *2.3.1. Quantum Chemical Calculations.* All binding energies (BEs) were corrected for basis set superposition errors (BSSE) estimated from the counterpoise method.[13]

a. Dimer Interactions. BEs for the $[CmOx]^+$ dimer in both side-on and end-on coordination are calculated for various Cm−Ox distances keeping the internal oxalate geometry fixed at the equilibrium geometry. For this step, the MP2 level of theory was employed as implemented in the MOLPRO software package, using diffuse aug-cc-pVTZ basis sets on all oxygen and hydrogen atoms, as well as an all-electron basis set of quadrupel-zeta quality for Cm.[14] All 1s oxygen electron orbitals and the 5d and lower energy orbitals for Cm(III) were kept frozen. Scalar relativistic effects were treated self-consistently using the second-order Douglas−Kroll−Hess Hamiltonian.

b. Cluster Formation. The BEs and geometries for all possible combinations of side-on and end-on coordination of $[Cm(Ox)_n]^{3-2n}$ (n = 0, 1, 2, 3, 4) forming a 9-fold coordinated Cm(III) ion were determined. Geometry optimizations were carried out using density functional theory (DFT) with the BP86 functional and a triple-ζ basis set on all atoms.[15,16] All structures were proven to be true minima by vibrational frequency calculation on the m5 grid. In a second step, BEs were obtained on the MP2 level of theory employing the resolution of the identity technique (RIMP2) as implemented in the TURBOMOLE software package.[17−19] As for the dimer interactions, all oxygen, hydrogen, and carbon atoms were described by aug-cc-pVTZ basis sets. A small-core relativistic pseudopotential (ECP60MWB) was used for the Cm(III) ion.[20]

2.3.2. Molecular Dynamics. Classical MD simulations were performed using the polarizable TCPEp force field implemented in the Polaris (MD) code.[21,22] For the water molecule only one point dipole is considered located on its oxygen atom with a polarizability value of 1.45 Å^3. No polarizable model has been proposed for the Ox^{2-} ion up to now. Hence, in the present work the static charges and polarizabilities were calculated by an atomic dipole moment corrected Hirshfeld [23−26] analysis on the DFT/aug-cc-pVTZ level using the B3-LYP functional [16], resulting in $q_O = -0.73$, $q_C = 0.45$, and isotropic polarizability values of α_O = 2.10 Å^3 and α_C= 1.25 Å^3. The O−C and C−C bonds as well as O−C−C and O−C−O angular potentials are constrained by a harmonic potential around their RIMP2 equilibrium values of 1.267 Å, 1.618 Å, 116.90°, and 126.19°, respectively.[23] No dihedral potential was applied as the charge−charge repulsion described the rotational potential sufficiently well.[24]

Simulations (10 ns) were carried out on a cubic box containing one Cm(III) ion and one to four Ox^{2-} ions solvated by 1000 H_2O molecules using periodic boundary conditions.[25] Fourteen trajectories were generated with starting points corresponding to the hydrated $[Cm(Ox)_n(H_2O)_m]^{3-2n}$ structures, which were optimized in the gas phase.[26] The NVT ensemble at ambient conditions (T = 300 K, water density 1 g/cm^3) was chosen, where equations of motion were solved using the r-RESPAp algorithm with two time steps of 1 fs (short-range interactions) and 5 fs (long-range interactions).[27] The temperature was modeled using a Gaussian moment thermostat.[28] Both the water O−H bonds and H−O−H angles were constrained using the iterative RATTLE procedure.[29] Statistical averages are computed from the last 9 ns of the trajectory, sampled at each 0.5 ps. The water/ligand-

DOI: 10.1021/ic502749x
Inorg. Chem. 2015, 54, 1860−1868

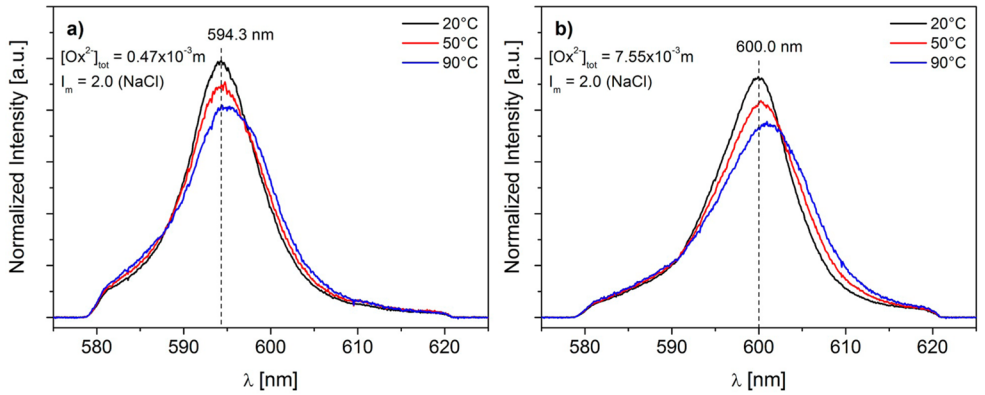

Figure 1. Normalized emission spectra of Cm(III) at $[H^+]_{tot} = 9.31 \times 10^{-3}$ m, $I_m = 2.0$ (NaCl), $T = 20$, 50, 90 °C, and (a) $[Ox^{2-}]_{tot} = 0.47 \times 10^{-3}$ m, (b) $[Ox^{2-}]_{tot} = 7.55 \times 10^{-3}$ m.

structure around the metal ions is investigated by computing standard radial distribution functions (RDFs) averaging over different trajectories from the corresponding end-on and side-on starting points. Analyzing the bond-length autocorrelation function proposed by Impey, a good statistics of the full configuration space is obtained after ∼3 ns of simulation.[30]

3. RESULTS AND DISCUSSION

3.1. Emission Spectra. The emission spectra of Cm(III) are recorded at different oxalate concentrations, ionic strengths, and temperatures up to 90 °C. The results show that the emission intensity of the fluorescence spectra decreases successively with increasing temperature by ∼70%. The decrease depends on the temperature and is independent of other experimental conditions ($[Ox^{2-}]_{tot}$, $[H^+]_{tot}$, I_m). The main reason for this effect is a thermal population of higher energetic levels of the Cm(III) ion and following nonradiative relaxation. Details are given elsewhere.[31] Thus, all emission spectra are normalized to equal integral to enhance comparability. As an example, the normalized emission spectra of Cm(III) at two different total oxalate concentrations and T = 20, 50, and 90 °C are given in Figure 1.

At $[Ox^{2-}]_{tot} = 0.47 \times 10^{-3}$ m and 20 °C an emission band at 594.3 nm is observed. Compared to the emission band of the Cm^{3+} aquo ion (593.8 nm[31]) this band is shifted by 0.5 nm to higher wavelength. This indicates that already at low ligand concentration Cm(III) oxalate species are formed. At increased temperatures the band is shifted further toward higher wavelengths, and a shoulder appears at ∼598.0 nm. At higher oxalate concentration and 20 °C the maximum of the emission band is located at 600.0 nm. This shows that the majority of the Cm(III) is complexed by oxalate, indicating the presence of $[Cm(Ox)_n]^{3-2n}$ ($n > 1$) complexes.

For all concentrations the emission band is generally shifted toward higher wavelengths with increasing temperature. Additionally, a minor hot band appears at ∼585 nm, resulting from the thermal population of higher energetic levels of the first excited state ($^5D'_{7/2}$). The temperature dependency of the emission spectra shows that the formation of the complexed species is favored at increased temperatures. A quantitative analysis of the spectra is given in the following section.

3.2. Peak Deconvolution and Speciation. In Figure 2 the single-component spectra of the different Cm(III)-oxalate species are shown. The single-component spectra of the $[Cm(Ox)_n]^{3-2n}$ species are shifted successively by ∼2.5 nm to higher wavelengths with each additional ligand. The spectra for

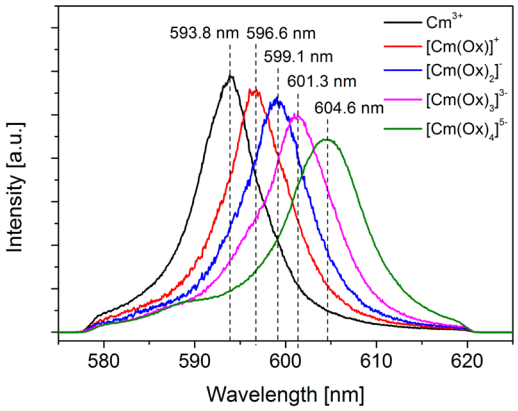

Figure 2. Single-component spectra of the species Cm^{3+} aquo ion (593.8 nm)), $[Cm(Ox)]^+$ (596.8 nm), $[Cm(Ox)_2]^-$ (599.1 nm), $[Cm(Ox)_3]^{3-}$ (601.3 nm), and $[Cm(Ox)_4]^{5-}$ (604.6 nm).

n = 1, 2, and 3 are determined at 20 °C. Since the $[Cm(Ox)_4]^{5-}$ complex forms only at elevated temperatures the spectrum for n = 4 was determined at 90 °C. Thus, a small hot band at ∼588 nm is visible in the single-component spectrum of this species. To derive the molar fractions of the different chemical species from the relative intensity ratios of the respective single-component spectra of the peak deconvolution, relative fluorescence intensity (FI) factors of the different species must be considered. Details on the FI factors are given in the Supporting Information. In the present work no systematic variation of the intensities of the Cm(III) spectra with increasing oxalate concentrations and T = constant are observed. Thus, differences in the FI factors of the $[Cm(Ox)_n]^{3-2n}$ complexes are negligible. Furthermore, a monoexponential decay of the FI is observed at all experimental conditions. This behavior is typical for systems where the exchange rate of the ligands is distinctively higher compared to the lifetime of the first excited state. In this case, the relative intensity ratios are governed by the thermodynamic equilibrium, and differences in the FI factors affect only the total emission intensity. This effect is discussed in detail elsewhere.[32,33] Thus, in the present work the FI factors are treated as unity.

The assignment of the single-component spectra to the respective Cm(III) oxalate species is verified by linear slope analysis. In the present work the slope analysis is performed at each studied ionic strength and each temperature by plotting

DOI: 10.1021/ic502749x
Inorg. Chem. 2015, 54, 1860−1868

the logarithm of $[Ox^{2-}]_{eq}$, $[HOx^{-}]_{eq}$, and $[NaOx^{-}]_{eq}$ versus $\log([Cm(Ox)_n]^{3-2n}/[Cm(Ox)_{n-1}]^{3-2(n-1)})$ (n = 1, 2, 3). The results show that linear fits are achieved solely by plotting $\log([Ox^{2-}]_{eq})$. Thus, only complexes with Ox^{2-} ($[Cm(Ox)_n]^{3-2n}$) are formed under the present experimental conditions. The complexation by the potential ligands HOx^{-} and $NaOx^{-}$ was not observed. This is in agreement with the literature data.[1] A plot of $\log([Ox^{2-}]_{eq})$ versus $\log([Cm(Ox)_n]^{3-2n}/[Cm(Ox)_{n-1}]^{3-2(n-1)})$ at T = 20 °C is given in Figure 3. Because of their large error, data points with at least one Cm(III) species being below 10% are not taken into account.

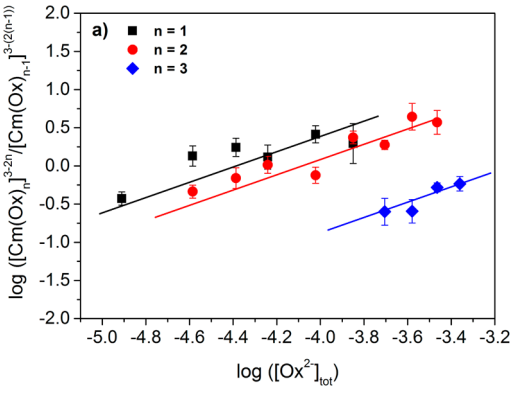

Figure 3. Plot of $\log([Cm(Ox)_n]^{3-2n}/[Cm(Ox)_{n-1}]^{3-2(n-1)})$ vs $\log([Ox^{2-}]_{eq})$ (n = 1, 2, 3) at T = 20 °C and I_m = 2.0. Lines represent a slope of 1.0.

Using the single-component spectra (see Figure 2) the speciation of each sample is determined as a function of $[Ox^{2-}]_{tot}$, I_m, and T. Two speciation plots at I_m = 1.0 and T = 20 and 90 °C are shown in Figure 4 as a function of $[Ox^{2-}]_{tot}$. For details on the speciation of each studied sample see the Supporting Information. At ambient temperatures and $[Ox^{2-}]_{tot} < 1.5 \times 10^{-3}$ m the speciation is determined mainly by the Cm^{3+} aquo ion and the $[Cm(Ox)]^{+}$ complex. The higher complexes are minor species under these conditions. At higher ligand concentration the $[Cm(Ox)_2]^{-}$ and $[Cm(Ox)_3]^{3-}$ complexes increase considerably, with the former complex being the dominant species. Furthermore, no $[Cm(Ox)_4]^{5-}$ complex is formed at these conditions.

At 90 °C the speciation changes significantly. The molar fraction of the Cm^{3+} aquo ion is slightly increased, while the formation of the $[Cm(Ox)]^{+}$ and $[Cm(Ox)_2]^{-}$ complexes is suppressed. No distinct impact of the temperature on the molar fraction of $[Cm(Ox)_3]^{3-}$ is observed. However, the formation of the $[Cm(Ox)_4]^{5-}$ complex increases strongly. This species is present to ~20% at the highest studied oxalate concentration.

3.3. Stability Constants and Thermodynamics. Using the calculated free oxalate concentrations and the concentrations of the different $Cm(Ox)_n^{3-2n}$ species, the conditional stability constants ($\log K'_n(T)$) are calculated according to the law of mass action (eq 1).

$$K'_n = \frac{[Cm(Ox)_n]^{3-2n}}{[Cm(Ox)_{n-1}]^{3-2(n-1)} \cdot [Ox]^{2-}} \quad (1)$$

These values are valid only for the respective ionic strength. Furthermore, the temperature-dependent change of the conditional stability constants results from two different effects. First, the change of the constant itself; second, the temperature-dependent change of the activity coefficients of the reactive species ($\gamma_i(T)$). Thus, to solely determine the temperature dependency of the stability constants, the conditional $\log K'_n(T)$ values are extrapolated to zero ionic strength, yielding the thermodynamic $\log K^0_n(T)$ values. This extrapolation is done by applying the specific ion interaction theory.[1] The $\log K^0_n(T)$ values are summarized in Table 1.

Table 1. $\log K^0_n(T)$ Values of the $[Cm(Ox)_n]^{3-2n}$ Complexes (n = 1, 2, 3, 4)

T [°C]	$\log K^0_1$	$\log K^0_2$	$\log K^0_3$	$\log K^0_4$
20	6.86 ± 0.03	4.68 ± 0.09	2.11 ± 0.05	
30	6.86 ± 0.06	4.71 ± 0.08	2.20 ± 0.10	
40	6.80 ± 0.14	4.71 ± 0.11	2.24 ± 0.07	
50	6.80 ± 0.18	4.78 ± 0.09	2.41 ± 0.10	
60	6.75 ± 0.07	5.01 ± 0.09	2.38 ± 0.10	1.08 ± 0.22
70	6.73 ± 0.09	5.00 ± 0.11	2.40 ± 0.07	0.71 ± 0.12
80	6.86 ± 0.06	4.96 ± 0.05	2.48 ± 0.06	0.73 ± 0.07
90	6.76 ± 0.04	5.03 ± 0.12	2.40 ± 0.07	0.72 ± 0.06

The $\log K^0_1(T)$ value changes slightly within the studied temperature range. The value decreases by ~0.10 orders of magnitude. However, this change is within the error range of the values. The change of the $\log K^0_2(T)$ and $\log K^0_3(T)$ values with the temperature is more pronounced. Both constants increase by ~0.33 logarithmic units in T = 20–90 °C. Since the $[Cm(Ox)_4]^{5-}$ complex exists only at higher temperatures, $\log K^0_4$ is determined at T > 50 °C. However, because of the large error of $\log K^0_4(T)$ these values should be treated with care.

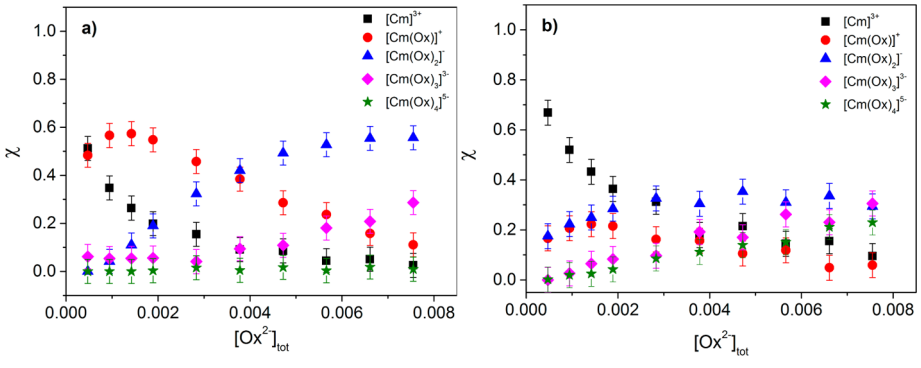

Figure 4. Molar fractions of the $[Cm(Ox)_n]^{3-2n}$ (n = 1, 2, 3, 4) complexes as a function of $[Ox^{2-}]_{tot}$ at I_m = 1.0, $[H^+]_{tot} = 9.31 \times 10^{-3}$ m and (a) T = 20 °C, (b) T = 90 °C.

DOI: 10.1021/ic502749x
Inorg. Chem. 2015, 54, 1860–1868

In the literature many studies on the complexation of actinides with oxalate at ambient temperatures are available. A critical review of the available data is given in the NEA TDB, giving values for log $K^0_{1,25\ °C}$ = 6.51 ± 0.15 and log $K^0_{2,25\ °C}$ = 4.20 ± 0.20.[1] However, an estimated log K^0_3 = 2.29 ± 1.0 is also given. This value is based on a single publication and should be treated with care. For comparison with the literature data, values of log $K^0_{1,25\ °C}$ = 6.86 ± 0.06, log $K^0_{2,25\ °C}$ = 4.70 ± 0.09, and log $K^0_{3,25\ °C}$ = 2.16 ± 0.10 are interpolated from the present data set for 25 °C. The results of the present work are in good agreement with the literature data. No literature data on the temperature dependency of thermodynamic stability constants of oxalate complexes with trivalent actinides are available. However, some studies on U(VI) and Np(V) oxalate complexes at T = 10−70 °C were performed.[34,35] DiBernardo et al. determined a value of log $K^0_{1,25\ °C}([UO_2(Ox)])$ = 7.44 ± 0.07. This value shows no clear temperature dependency up to 70 °C.

The log $K^0_{2,25\ °C}([UO_2(Ox)_2]^{2-})$ = 4.63 ± 0.10 and log $K^0_{3,25\ °C}([UO_2(Ox)_3]^{4-})$ = 1.33 ± 0.25 increase by 0.2 and 0.4 orders of magnitude with increasing temperature. Regarding the chemical differences of Cm(III) and U(VI), the temperature dependencies of the log K values of U(VI)-oxalate complexes agree with the present results.

The log $K^0_n(T)$ (n = 1, 2, 3) are linearly correlated with the reciprocal temperature. Thus, $\Delta_r H^0_m$ = constant and $\Delta_r C^0_{p,m}$ = 0 are assumed in the studied temperature range, and the temperature dependency of the thermodynamic stability constants is fitted by the integrated Van't Hoff equation (eq 2).

$$\log \beta^0_n(T) = \log \beta^0_n(T_0) + \frac{\Delta_r H^\circ(T_0)}{R\cdot\ln(10)}\cdot\left(\frac{1}{T_0} - \frac{1}{T}\right) \quad (2)$$

The plots of the log $K^0_n(T)$ values versus the reciprocal temperature are given in Figure 5. Also, the log $K^0_4(T)$ values

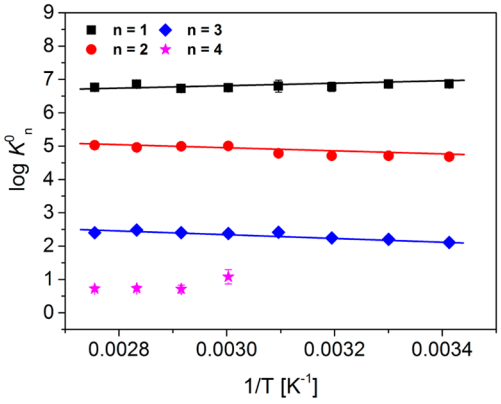

Figure 5. log K^0_n (n = 1, 2, 3,4) as a function of 1/T. Linear fits according to the integrated van't Hoff equation (eq 2).

are shown. Because of the limited number of data points we refrained from fitting these data according to eq 2. The $\Delta_r H^0_m$ and $\Delta_r S^0_m$ values are given in Table 2.

The results show a small exothermic standard reaction enthalpy for the formation of the $[Cm(Ox)]^+$ complex. This is a strong indication that the ligand is coordinated to the metal ion via both carboxylic groups forming a five-membered chelate ring (side-on coordination). Since five- and six-membered rings are among the most stable ring structures in chemistry, the formation of a chelating ring results in a high binding energy

Table 2. Standard Reaction Enthalpy ($\Delta_r H^0_m$) and Entropy ($\Delta_r S^0_m$) of the Stepwise Formation of $[Cm(Ox)_n]^{3-2n}$ Complexes (n = 1, 2, 3)

$CmOx_{n-1}^{3-2(n-1)} + Ox^{2-} \leftrightarrow CmOx_n^{3-2n}$	$\Delta_r H^0_m$ [kJ/mol]	$\Delta_r S^0_m$ [J/mol·K]
n = 1	−2.7 ± 0.8	121.8 ± 2.9
n = 2	10.8 ± 1.8	126.0 ± 3.2
n = 3	10.3 ± 1.5	76.0 ± 3.1

and thus leads to an overall exothermic complexation reaction.[36] The side-on coordination mode is confirmed by the quantum chemical calculations (see Section 4). On the contrary, the stepwise formation of $[Cm(Ox)_2]^-$ and $[Cm(Ox)_3]^{3-}$ are both endothermic, with similar values for $\Delta_r H^0_m$. However, the quantum chemical calculations also show a side-on coordination of these two ligands. The endothermic reaction enthalpies are thus explained by the change of the charge of the complex from positive to negative in these two reaction steps. This leads to an electrostatic repulsion of the ligand, and less energy is released in the complexation step. The standard reaction entropies of the first three complexation steps are all positive. The $\Delta_r S^0_m$ for n = 1 and 2 show similar values of ~123 J/mol·K. The $\Delta_r S^0_m$ of the formation of $[Cm(Ox)_3]^{3-}$ is ~50 J/mol·K lower. Thus, the formation of the $[Cm(Ox)]^+$ complex is both enthalpy and entropy driven, while the driving force of the $[Cm(Ox)_2]^-$ and $[Cm(Ox)_3]^{3-}$ complexes is the gain in reaction entropy. The determined reaction entropies indicate that fewer degrees of freedom are gained by the system in the third complexation step compared to the first and second steps. This can be attributed to a more rigid structure of the $[Cm(Ox)_3]^{3-}$ complex, which results in less conformational isomers for this complex. The higher rigidity of the $[Cm(Ox)_3]^{3-}$ complex is confirmed by the quantum chemical calculations (for more details see Section 4.2.2). Furthermore, although no thermodynamic data are determined for the formation of the $[Cm(Ox)_4]^{5-}$ complex, the fact that this complex appears only at higher temperatures is a strong indication that this complexation step is also endothermic and strongly driven by the reaction entropy. Unfortunately, no literature data on trivalent actinides are available for comparison. Furthermore, the data given by DiBernardo et al. on U(VI) oxalate complexes are valid for $[NaClO_4]$ = 1.05 m and cannot be compared with the present results.

3.4. Binary Ion−Ion Interaction Coefficients. By plotting log $K'_n(T) - \Delta z^2 D$ versus the ionic strength and using the linear fitting of the data points, the binary ion−ion interaction coefficients ($\varepsilon(i,k)$) of the $[Cm(Ox)_n]^{3-2n}$ complexes were determined. Thereby D is the Debye−Hückel term and $\Delta z^2 = \sum z_{end}{}^2 - z_{start}{}^2$. The $\Delta\varepsilon_n$ (n = 1, 2, 3, 4) values are summarized in Table 3. Because of the limited number of data for the formation of the $[Cm(Ox)_4]^{5-}$ complex, errors of these values are relatively high. The $\Delta\varepsilon_n$ data shows no distinct change with increasing temperature. This is in good agreement with the literature.[1] In general, the values for $(\partial\varepsilon/\partial T)$ are ≤0.005 kg·mol^{-1}·K^{-1} for temperatures below 473 K. Furthermore, the $(\partial\varepsilon/\partial T)$ for the products and reactants may balance out each other, so that $\Delta\varepsilon_n(T)$ remains constant.[37]

Thus, the following temperature-independent $\Delta\varepsilon_n$ values are determined by averaging the data obtained in the studied temperature range: $\Delta\varepsilon_1$ = −0.205 ± 0.025, $\Delta\varepsilon_2$ = −0.115 ± 0.045, $\Delta\varepsilon_3$ = −0.061 ± 0.040, $\Delta\varepsilon_4$ = 0.162 ± 0.200. By using these values and $\varepsilon_{25\ °C}(Cm^{3+},Cl^-) \approx \varepsilon_{25\ °C}(Am^{3+},Cl^-)$ = 0.23 ± 0.02 and $\varepsilon_{25\ °C}(Na^+,Ox^{2-})$ = −0.08 ± 0.01 given by the NEA-

DOI: 10.1021/ic502749x
Inorg. Chem. 2015, 54, 1860−1868

Table 3. $\Delta\varepsilon_n(T)$ Values for the Stepwise Formation of the $[Cm(Ox)_n]^{3-2n}$ Complexes (n = 1, 2, 3, 4)

T [°C]	$\Delta\varepsilon_1$	$\Delta\varepsilon_2$	$\Delta\varepsilon_3$	$\Delta\varepsilon_4$
20	−0.206 ± 0.008	−0.107 ± 0.032	−0.078 ± 0.017	
30	−0.201 ± 0.019	−0.102 ± 0.029	−0.074 ± 0.032	
40	−0.218 ± 0.047	−0.107 ± 0.035	−0.080 ± 0.039	
50	−0.210 ± 0.014	−0.115 ± 0.030	−0.060 ± 0.031	
60	−0.223 ± 0.017	−0.077 ± 0.031	−0.071 ± 0.028	(0.292 ± 0.185)
70	−0.208 ± 0.012	−0.100 ± 0.038	−0.056 ± 0.021	(0.168 ± 0.144)
80	−0.164 ± 0.022	−0.145 ± 0.020	−0.032 ± 0.018	(0.159 ± 0.124)
90	−0.201 ± 0.015	−0.136 ± 0.042	−0.064 ± 0.023	(0.154 ± 0.124)

TDB[1], the binary $\varepsilon(Cm(Ox)_n^{3-2n}, Cl^-/Na^+)$ values for the different species are calculated. The results are given in Table 4.

Table 4. Binary Ion−Ion Interaction Parameters for the $[Cm(Ox)_n]^{3-2n}$ Complexes (n = 1, 2, 3, 4)

$\varepsilon(Cm(Ox)^+,Cl^-)$	−0.06 ± 0.04	p.w.[a]
$\varepsilon(Cm(Ox)_2^-,Na^+)$	−0.26 ± 0.06	p.w.
$\varepsilon(Cm(Ox)_3^{3-},Na^+)$	−0.40 ± 0.10	p.w.
$\varepsilon(Cm(Ox)_4^{5-},Na^+)$	−0.32 ± 0.30	p.w.
$\varepsilon(Am(Ox)^+,ClO_4^-)$	0.08 ± 0.10	ref 1
$\varepsilon(Am(Ox)_2^-,Na^+)$	−0.21 ± 0.10	ref 1
$\varepsilon(Am(Ox)_3^{3-},Na^+)$[b]	−0.23 ± 0.10	ref 1

[a]p.w. indicates data from the present work. [b]Approximated by $\varepsilon(Am(Ox)_3^{3-},Na^+) \approx \varepsilon(Am(CO_3)_3^{3-},Na^+)$.

The results show a constant decrease of the interaction coefficients with increasing number of oxalate ligands in the inner coordination sphere. This trend is in good agreement with the general trend observed for $\varepsilon(i,k)$ values of successive complexes.[1]

In the NEA-TDB no value for $\varepsilon(Am(Ox)^+,Cl^-)$ is given, whereas $\varepsilon(Am(Ox)^+,ClO_4^-)$ = 0.08 ± 0.10 is available. This value is higher compared to $\varepsilon(Cm(Ox)^+,Cl^-)$ determined in the present work. This is in good agreement with other data in the literature, since ion−ion interactions coefficients of cationic species with ClO_4^- are in general higher than those with Cl^-.[1] The here-determined $\varepsilon(Cm(Ox)_2^-,Na^+)$ = −0.26 ± 0.06 is in good agreement with the literature value for Am^{3+}. The value for $\varepsilon(Cm(Ox)_3^{3-},Na^+)$ = −0.40 ± 0.10 is distinctively higher than the value for $\varepsilon(Am(Ox)_3^{3-},Na^+)$. The reason for this deviation might be the fact that the value for $\varepsilon(Am(Ox)_3^{3-},Na^+)$ = −0.23 ± 0.10 is determined by estimation using the correlation $\varepsilon(Am(Ox)_3^{3-},Na^+) \approx \varepsilon(Am(CO_3)_3^{3-},Na^+)$. Furthermore, the given $\varepsilon(Am(Ox)_3^{3-},Na^+)$ is similar to $\varepsilon(Am(Ox)_2^-,Na^+)$. This does not fit to the general trend for decreasing $\varepsilon(i,k)$ values of complexes of a metal cation with increasing numbers of anionic ligands. The results of the present work are in far better agreement with this general trend for $\varepsilon(i,k)$ values. No literature data are available for comparison regarding the $[Cm(Ox)_4]^{4-}$ complex.

4. STRUCTURE AND COORDINATION MODES OF THE $Cm(Ox)_n^{3-2n}$ COMPLEXES

The question arises in which coordination mode the Ox^{2-} ligands bind to the Cm(III) ion. The here-determined emission bands of the individual complexes are comparable to the bands of the corresponding Cm(III) acetate and propionate complexes.[12,38,39] These ligands bind in a bidentate, non-chelating coordination mode (end-on) to the metal ion. Thus, the shift of the single-component spectra of the $[Cm(Ox)_n]^{3-2n}$ complexes suggests a binding of oxalate via one carboxylic group. However, the complexation strength and the associated stability constants of the Cm(III) oxalate complexes are by 3 orders of magnitude higher compared to acetate or propionate. This rather points toward a chelating coordination of oxalate via two oxygen atoms, one from each of the deprotonated

Table 5. Calculated Binding Energies (BE) and Cm(III)−O_{H2O}, Cm(III)−O_{Ox}, and Cm(III)−C_{Ox} Distances for the Complexes $[Cm(Ox)_n]^{3-2n}$ (n = 1, 2, 3, 4) in the Gas Phase

conformation	BE [kJ/mol]	distance [Å] Cm(III)−O_{H2O}	distance [Å] Cm(III)−O_{Ox}		distance [Å] Cm(III)−C_{Ox}	
			side-on	end-on	side-on	end-on
$[Cm(H_2O)_9]^{3+}$	−2209.8	2.54				
$[Cm(H_2O)_7(Ox^b)]^+$	−4353.9	2.57	2.39		3.22	
$[Cm(H_2O)_7(Ox^a)]^+$	−4257.9	2.55		2.44		2.74
$[Cm(H_2O)_5(Ox^b)_2]^-$	−6285.1	2.60	2.43		3.27	
$[Cm(H_2O)_5(Ox^b)(Ox^a)]^-$	−6211.8	2.56	2.40	2.50	3.23	2.82
$[Cm(H_2O)_5(Ox^a)_2]^-$	−6116.4	2.52		2.50		2.77
$[Cm(H_2O)_3(Ox^b)_3]^{3-}$	−7986.7	2.57	2.49		3.32	
$[Cm(H_2O)_3(Ox^b)_2(Ox^a)]^{3-}$	−7888.0	2.58	2.46	2.49	3.09	2.83
$[Cm(H_2O)_3(Ox^b)(Ox^a)_2]^{3-}$	−7840.7	2.60	2.44	2.51	3.27	2.84
$[Cm(H_2O)_3(Ox^a)_3]^{3-}$	−7766.7	2.59		2.49		2.81
$[Cm(H_2O)(Ox^b)_4]^{5-}$	−9528.9	2.69	2.51		3.33	
$[Cm(H_2O)(Ox^b)_3(Ox^a)]^{5-}$	−9372.9	2.68	2.49	2.60	3.31	2.92
$[Cm(H_2O)(Ox^b)_2(Ox^a)_2]^{5-}$	−9291.9	2.66	2.47	2.60	3.28	2.93
$[Cm(H_2O)(Ox^b)(Ox^a)_3]^{5-}$	−9199.2	2.64	2.45	2.56	3.26	2.88
$[Cm(H_2O)(Ox^a)_4]^{5-}$	−9093.1	2.63		2.53		2.85

[a]End-on coordination. [b]Side-on coordination.

DOI: 10.1021/ic502749x
Inorg. Chem. 2015, 54, 1860−1868

carboxylic groups (side-on). To gain a deeper insight into the interactions of Cm(III) and the oxalate ligand a series of quantum chemical calculations is performed.

4.1. Gas-Phase Results. The structures and BEs of the $[Cm(Ox)_n]^{3-2n}$ (n = 1, 2, 3, 4) complexes are calculated in the gas phase. Hereby, all possible combinations of end-on and side-on coordination modes of the ligands are considered. The results are given in Table 5. The bond lengths of Cm(III) to the oxygen atoms of the oxalate ligand are significantly shorter compared to the corresponding oxygen atoms of water in the first coordination sphere. Also, the side-on coordination of oxalate results in shorter Cm(III)−O_{Ox} bond lengths (2.39 to 2.51 Å), whereas the end-on coordination leads to bond lengths of 2.44 to 2.60 Å.

For all calculated complexes the lowest BSSE-corrected BEs are found for the structures where every ligand is bound in a side-on coordination mode. Furthermore, the binding energies of the various complexes increase with the amount of end-on coordination. This trend is explained by the higher stability of the five-membered chelating ring compared to the four-membered ring, which forms upon the coordination of an oxalate ligand via a single carboxylic group (end-on). These findings strongly indicate that oxalate binds to Cm(III) in a chelating mode via two oxygen atoms, one of each carboxylic group.

4.2. Molecular Dynamics Studies. A better comparability with the experimental results is achieved by application of molecular dynamics simulations. Hereby, the different Cm(III) oxalate complexes are calculated in a virtual box containing 1000 H_2O molecules. The parameters of the Cm(III)−oxalate−H_2O force field were adjusted to 350 ab initio reference points using a simulated annealing technique coupled with the PEST parameter optimizer.[40] A mean error of 18.84 kJ/mol for the FF energies compared to the reference data was achieved. Details on the force field are given in the Supporting Information.

4.2.1. Bond Lengths. The calculated bond distances for the different complexes are given in Table 6. The radial distribution functions of the different systems are given in the Supporting Information.

Table 6. Cm(III)−O_{H2O}, Cm(III)−O_{Ox}, and Cm(III)−C_{Ox} Bond Distances for the Complexes $[Cm(Ox)_n]^{3-2n}$ (n = 1, 2, 3, 4) Calculated by MD Simulations

conformation	distance [Å] Cm(III)−O_{H2O}	distance [Å] Cm(III)−O_{Ox}	distance [Å] Cm(III)−C_{Ox}
$[Cm(Ox^a)]^+$	2.40	2.51	2.80
$[Cm(Ox^a)_2]^-$	2.43	2.53	2.93
$[Cm(Ox^a)_3]^{3-}$	2.43	2.57	2.98
$[Cm(Ox^a)_2(Ox^b)]^{3-}$	2.42	2.53	2.94

[a]Side-on coordination. [b]End-on coordination.

For the $[Cm(Ox)]^+$ complex a side-on coordination was found along the MD trajectories independent of the starting configuration. When an end-on configuration is used as the starting structure it transforms into the side-on mode after 0.3 ns. For the $[Cm(Ox)_2]^-$ complex all starting structures resolved in an all side-on coordination. The corresponding bond distances are slightly longer compared to the $[Cm(Ox)]^+$ complex, which is in good agreement with the gas-phase results. For the $[Cm(Ox)_3]^{3-}$ complex two conformations are stable within the time frame of the MD simulation (10 ns). These two conformations are the all side-on (3s) and the two side-on and one end-on (2s1e) structures. However, the average energy of the 3s structure is by 201 kJ/mol lower compared to the 2s1e conformation. Furthermore, the 3s conformation forms exclusively when the starting structure does not a priori contain a 1:3 complex but rather the ligands approach the Cm(III) ion from afar along the MD trajectory. The bond distances of the 3s configuration are slightly longer compared to the 2s1e configuration. Regarding the $[Cm(Ox)_4]^{5-}$ complex none of the gas-phase optimized structures were stable. Within the time frame of 10 ns one of the four ligands exchanged into the second or third hydration shell and was replaced by two H_2O molecules. This is in good agreement with the experimental results, where the 1:4 complex was observed only at elevated temperatures. These findings further support that all oxalate ligands bind in a side-on coordination mode toward the Cm(III) ion.

4.2.2. Bond Angles. A slight distortion of the internal geometry of the oxalate ion is observable upon coordination to the Cm(III) ion. This effect is shown by comparison of the two Cm−C−O angles a and b (see Figure 6).

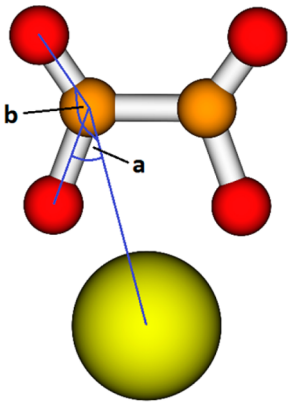

Figure 6. Cm−C−O angles a and b within the Cm(III)-oxalate entity.

The angular distribution functions for these four structures are given in Figure 7. For the $[Cm(Ox)]^+$ complex in the gas phase these angles are a = 34.9° and b = 160.2°. Along the MD trajectory two maxima are determined at a = 59.0° and b = 158.8°. This shows a bending of the oxalate ion upon complexation. This bending is also observable for the

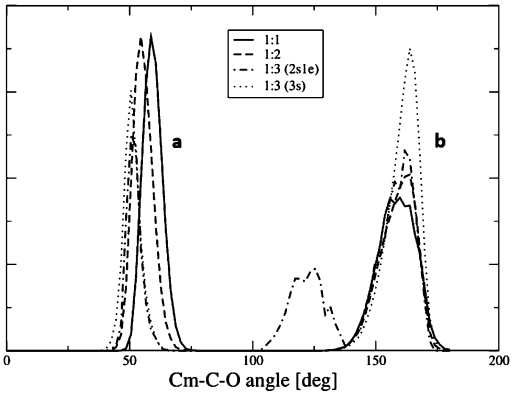

Figure 7. Angular distribution functions of the Cm−C−O angles a and b.

DOI: 10.1021/ic502749x
Inorg. Chem. 2015, 54, 1860−1868

$[Cm(Ox)_2]^-$ complex but less pronounced with $a = 54.8°$ and $b = 161.2°$.

Regarding the $[Cm(Ox)_3]^{3-}$ complex in the 3s conformation comparable results are determined with $a = 50.9°$ and $b = 164.4°$. Also, for the 2s1e conformation these two angles are similar ($a = 51.4°$, $b = 162.6°$). Here, an additional maximum is found at 122.2°. This peak originates from the noncoordinating oxygens of the end-on coordinated oxalate ion.

Furthermore, a twisting of the O−C−C−O dihedral angle of oxalate is observable upon complexation. This allows the oxalate ligand to adjust to changes in the water hydrogen bond network. The distribution of the dihedral angles is given in Figure 8.

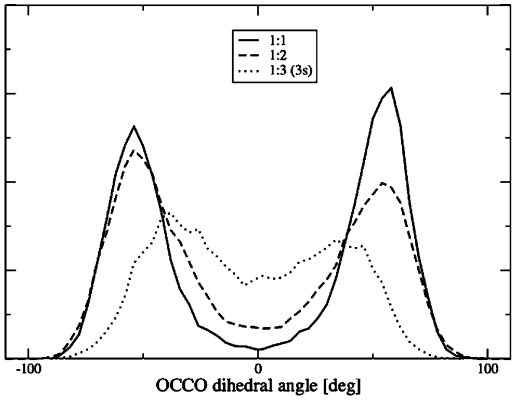

Figure 8. Distribution of the O−C−C−O dihedral angle of the side-on coordinated oxalate ligand.

For the $[Cm(Ox)]^+$ complex the results show a value of ±56.1°. For the $[Cm(Ox)_2]^-$ complex the dihedral screw is slightly smaller due to the presence of the second ligand with a maximum at ±54.3°. The presence of a third ligand in the $[Cm(Ox)_3]^{3-}$ restricts the dihedral motion significantly, resulting in a value of ±38.7°. This restriction leads to a more rigid structure of the $[Cm(Ox)_3]^{3-}$ complex, explaining the lower reaction entropy of the third complexation step (see Table 2).

5. SUMMARY AND CONCLUSION

The present work is a detailed experimental and theoretical study on the thermodynamics and the structural properties of the $[Cm(Ox)_n]^{3-2n}$ ($n = 1, 2, 3$) complexes at $T = 20-90$ °C. The determined log $K^0_{n,25\ °C}$ values ($n = 1, 2, 3$) are in very good agreement with the NEA Thermodynamic Database. The results show that the changes of the thermodynamic stability constants with increasing temperature are small. The log $K^0_1(T)$ decreases by 0.1 orders of magnitude. Contrary to this, the log $K^0_2(T)$ and log $K^0_3(T)$ increase by ∼0.3 in the studied temperature range. The temperature-dependent thermodynamic stability constants are fitted with the integrated Van't Hoff equation, yielding the $\Delta_r H^0_m$ and $\Delta_r S^0_m$ values. The results show an exothermic reaction enthalpy for the first complexation step, while the two following steps are both endothermic. Furthermore, the binary ion−ion interaction coefficients of the different $[Cm(Ox)_n]^{3-2n}$ species are determined. The quantum chemical calculations confirmed that the oxalate ligand binds in a side-on coordination mode to the Cm(III) ion and forms a five-membered chelate ring. Additionally, the bond lengths and angles of the different Cm(III) oxalate species were calculated, gaining a deep insight into the structure of these complexes.

The data of the present work contribute to a better understanding and description of the complexation behavior of trivalent actinides with oxalate in the temperature range from 20 to 90 °C. Because oxalate salts have broad application in the nuclear fuel cycle and are present in nuclear waste repositories, these data are of high relevance for the modeling of the migration behavior of trivalent actinides under near field conditions; this study is therefore a valuable contribution to a comprehensive long-term safety assessment of nuclear waste repositories in deep geological formations.

■ ASSOCIATED CONTENT

Supporting Information

Discussion of pH values used in calculations, fluorescence intensity factors, tabulated data indicating speciation at 20, 30, 40, 50, 60, 70, 80, and 90 °C, conditional stability constants, force-field parameters used in molecular dynamics simulations, radial distribution functions. This material is available free of charge via the Internet at http://pubs.acs.org.

■ AUTHOR INFORMATION

Corresponding Author

*E-Mail: andrej.skerencak@kit.edu. Fax: +49 (0)721 608 23927. Phone: +49 (0)721 602 26024.

Notes

The authors declare no competing financial interest.

■ ACKNOWLEDGMENTS

This work was partially funded by the German Federal Ministry of Economics and Technology (BMWi) under Contract No. 02E11031. We acknowledge access to the computing resources provided by the Steinbuch Centre for Computing (SCC) at KIT.

■ REFERENCES

(1) Hummel, W.; Anderegg, G.; Puigdomenech, I.; Rao, L.; Tochiyama, O. *Chemical Thermodynamics of Compounds and Complexes of U, Np, Pu, Am, Tc, Se, Ni and Zr with Selected Organic Ligands;* OECD, NEA-TDB: North Holland, Amsterdam, 2005.

(2) Dollimore, D. *Thermochim. Acta* **1987**, *117*, 331−363.

(3) Arab-Chapelet, B.; Grandjean, S.; Nowogrocki, G.; Abraham, F. *J. Alloys Compd.* **2007**, *444*−*445*, 387−390.

(4) Machuron-Mandard, X.; Madic, C. *J. Alloys Compd.* **1996**, *235*, 216−224.

(5) Crawford B. A.; Lott S. A.; Sparks L. D.; Van Soest G.; McInroy B. The road to recertification: WIPP TRU Waste Inventory, *Proceedings of Waste Management 2006 Conference;* February 26−March 2, Tucson, Arizona, WMS: Tempe, AZ, 2006.

(6) Gammons, C. H.; Wood, S. A. *Chem. Geol.* **2000**, *166*, 102−124.

(7) Alderighi, L.; Gans, P.; Ienco, A.; Peters, D.; Sabatini, A.; Vacca, A. *Coord. Chem. Rev.* **1999**, *184*, 311−318.

(8) Daniele, P. G.; Rigano, C.; Sammartano, S. *Thermochim. Acta* **1981**, *46*, 103−116.

(9) Daniele, P. G.; Rigano, C.; Sammartano, S. *Thermochim. Acta* **1983**, *62*, 101−112.

(10) Daniele, P. G.; de Robertis, A.; Sammartano, S.; Rigano, C. *Thermochim. Acta* **1984**, *72*, 305−322.

(11) Puigdomenech, I.; Rard, J. A.; Plyasunov, A. V.; Grenthe, I. Temperature Corrections to Thermodynamic Data and Enthalpy Calculations. In *Modelling in Aquatic Chemistry;* Grenthe, I., Puigdomenech, I., Eds.; OECD, Nuclear Energy Agency: Paris, 1997.

(12) Fröhlich, D. R.; Skerencak-Frech, A.; Morkos, M. L. K.; Panak, P. J. *New. J. Chem.* **2013**, *37*, 1520−1528.

DOI: 10.1021/ic502749x
Inorg. Chem. 2015, 54, 1860−1868

(13) Boys, S. F.; Bernardi, F. *Mol. Phys.* **1970**, *19*, 553−566.
(14) Werner H. J., Knowles P. J., Knizia G., Manby F. R., Schütz M. et al. MOLPRO, version 2012.1, a package of ab initio programs, 2012; available at http://www.molpro.net/.
(15) Perdew, J. P. *Phys. Rev. B* **1986**, *33*, 8822−8824.
(16) Becke, A. D. *J. Chem. Phys.* **1993**, *98*, 5648−5652.
(17) Weigend, F.; Häser, F. *Theor. Chim. Acc.* **1997**, *97*, 331−340.
(18) Weigend, F.; Häser, F.; Patzelt, H.; Ahlrichs, R. *Chem. Phys. Lett.* **1998**, *294*, 143−152.
(19) TURBOMOLE V6.6 2014, a development of University of Karlsruhe and Forschungszentrum Karlsruhe GmbH, 1989.2007, TURBOMOLE GmbH, since 2007; available at http://www.turbomole.com.
(20) Küchle, W.; Dolg, M.; Stoll, H.; Preuss, H. *J. Chem. Phys.* **1994**, *100*, 7535−7542.
(21) Masella, M.; Flament, J. P. *J. Chem. Phys.* **1997**, *107*, 9105−9116.
(22) Masella, M.; Cuniasse, P. *J. Chem. Phys.* **2003**, *119*, 1866−1873.
(23) Hirshfeld, F. L. *Theor. Chim. Acta* **1977**, *44*, 129−138.
(24) Marenich, A. V.; Cramer, C. J.; Truhlar, D. G. *Chem. Sci.* **2013**, *4*, 2349−2356.
(25) Lu, T.; Chen, F. *J. Theor. Comput. Chem.* **2012**, *11*, 163−183.
(26) Lee, C.; Yang, W.; Parr, R. G. *Phys. Rev. B* **1988**, *37*, 785−789.
(27) Masella, M. *Mol. Phys.* **2006**, *104*, 415−428.
(28) Liu, Y.; Tuckerman, M. E. *J. Chem. Phys.* **2000**, *112*, 1685−1700.
(29) Martyna, G. J.; Tuckerman, M. E.; Tobias, D. J.; Klein, M. L. *Mol. Phys.* **1996**, *87*, 1117−1157.
(30) Impey, R. W.; Madden, P. A.; McDonald, I. R. *J. Phys. Chem.* **1983**, *87*, 5071−5083.
(31) Tian, G.; Edelstein, N. M.; Rao, L. *J. Phys. Chem. A* **2011**, *115*, 1933−1938.
(32) Edelstein, N. M.; Klenze, R.; Fanghänel, Th.; Hubert, S. *Coord. Chem. Rev.* **2006**, *250*, 948−973.
(33) Fanghänel, Th.; Kim, J. I. *Coord. Chem. Rev.* **1998**, *271*−*273*, 728−737.
(34) Di Bernardo, P.; Zanonato, P. L.; Tian, G.; Tolazzi, M.; Rao, L. *Dalton Trans.* **2009**, *23*, 4450−4457.
(35) Tian, G.; Rao, L. *Dalton Trans.* **2012**, *41*, 448−452.
(36) Panak, P. J.; Geist, A. *Chem. Rev.* **2013**, *113*, 119−1236.
(37) Plyasunov, V.; Grenthe, I. *Geochim. Cosmochim. Acta* **1994**, *58*, 3561−3582.
(38) Skerencak, A.; Höhne, S.; Hofmann, S.; Marquardt, C. M.; Panak, P. J. *J. Sol. Chem.* **2013**, *42*, 1−17.
(39) Fröhlich, D. R.; Skerencak-Frech, A.; Panak, P. J. *Dalton Trans.* **2014**, *43*, 3958−3965.
(40) Doherty J. Pest: Model-Independant Parameter Estimation and Uncertainty Analysis, 2010; available at http://www.pesthomepage.org.

DOI: 10.1021/ic502749x
Inorg. Chem. 2015, 54, 1860−1868